physica status solidi rrl
www.pss-rapid.com

Role of Intrinsic Surface States in Efficiency Attenuation of GaN-Based Micro-Light-Emitting-Diodes

*Fulong Jiang, Byung-Ryool Hyun, Yi Zhang, and Zhaojun Liu**

The effects of an intrinsic nonpolar surface on internal quantum efficiency (IQE) are numerically investigated for gallium nitride (GaN)-based micro-light emitting-diodes (μ-LEDs). It is found that due to the modulation of the surface density of states, the surface energy band bends upward, and valence band holes are naturally pushed toward the surface and are accumulated at the surface, resulting in significant nonradiative recombination. Consequently, the intrinsic surface states remarkably affect the IQE of μ-LEDs with a size of less than 30 μm due to the large surface-to-volume ratio, whereas the IQE of devices with a size of more than 30 μm is relatively insensitive to the intrinsic surface states. IQE starts to decrease for devices with a size of 30 μm, even without considering sidewall damage. In particular, starting from a size of 10 μm, μ-LEDs suffer a significant efficiency loss and the peak current density shifts to a higher value. The results open the way to improving device performance of μ-LEDs down to 1 μm and beyond, by incorporating surface band engineering combined with surface passivation over the full range of microdisplay applications.

In recent years, GaN-based micro-light-emitting-diodes (μ-LEDs) have emerged as the next-generation displays due to their excellent properties over liquid crystal displays (LCDs) and organic light-emitting diodes (OLEDs) such as high brightness, fast response, and low power consumption.[1–5] These features make them a most promising platform in high-end display applications such as mobile phones, wearable watches, augmented reality(AR)/virtual reality (VR) displays, which need high luminance, high pixel per inch (ppi), and high refresh rates.[1,4,5] Especially for the AR/VR displays, the shorter viewing distance (≈60 mm) requires a 1455 ppi because of the human eye resolution acuity of about 60 pixels per degree.[3] Such a high ppi necessitates the subpixel size to be shrunken down to a few micrometers (<5 μm).[1] In such a small size range, the external quantum efficiency (EQE) of μ-LEDs shows a significant reduction and the current density for the peak EQE shifts to higher values.[6] Thus, μ-LEDs with a size of less than 5 μm may not meet the requirement for the minimum peak brightness in AR/VR display applications.[1]

Recently, it has been reported that chemical treatment and sidewall passivation eliminate the size-dependent efficiency decrease for μ-LEDs with a size down to 10 μm.[7,8] However, μ-LEDs with a size smaller than 10 μm still suffer severe efficiency loss even with chemical treatments and passivation.[6] The previous studies have shown that the decreased EQE of μ-LEDs with size was attributed to the increased nonradiative surface recombination with decreasing size.[9–15] Therefore, extensive studies have been devoted to remove nonradiative recombination centers in the fabrication process of μ-LEDs and, as a result, dramatic improvements of the EQE have been achieved.[16] For example, using a combination of KOH chemical treatment and atomic layer deposition (ALD) for sidewall passivation, the EQE of μ-LEDs ranging from 10 to 100 μm reached about 23% with size independency.[7] Chemical treatments using KOH or TMAH solution have been performed to reduce the sidewall damage of GaN-based μ-LEDs induced from the inductively coupled plasma etching process. Nevertheless, the EQEs of μ-LED with a size smaller than 30 μm are still far below the efficiency of blue LEDs for solid-state lighting (SSL) (≈80%).[17] Recently, Smith et al. utilized an ingenious fabrication process to achieve μ-LEDs with size down to 1 μm, and the EQEs of the fabricated blue μ-LEDs begin to reduce significantly from sizes below 10 μm even though the sidewall damage was removed.[6] Thus, external effects are supposed to be very small on the observed EQE reduction. The modified ABC model introducing the surface recombination velocity multiplied by the coefficient of the surface–volume ratio was used to explain qualitatively the observed variation tendency.[6] However, the physical mechanism of efficiency loss in μ-LEDs is still unclear.

Further, for nitride materials, the surface recombination velocity is much smaller than that of AlGaInP materials, as well as the ambipolar diffusion coefficient of the nonequilibrium carrier with a value of about 1.7 $cm^2 s^{-1}$.[10,18] The diffusion length of the excitons for nitride materials is about 200 nm.[19] Thus, for GaN-based μ-LEDs, carrier diffusion from bulk to the surface should not cause such a big efficiency attenuation. Motivated by these initial results and physical properties of nitride materials, the intrinsic surface effect on the efficiency loss of μ-LEDs is studied in the wide size range of 1–300 μm. Our results show that

Dr. F. Jiang, Prof. B.-R. Hyun, Prof. Z. Liu
Department of Electrical and Electronic Engineering
Southern University of Science and Technology
Shenzhen 518055, China
E-mail: liuzj@sustech.edu.cn

Prof. Y. Zhang
Institute of Photoelectric Thin Film Devices and Technology
Nankai University
Tianjin 300350, China

The ORCID identification number(s) for the author(s) of this article can be found under https://doi.org/10.1002/pssr.202000487.

DOI: 10.1002/pssr.202000487

the upward bending of surface energy gives rise to the hole accumulation near the surface, leading to nonradiative surface recombination and thus, causing significant efficiency loss in small-sized (<10 μm) devices.

Considering the application of μ-LEDs to microdisplays, the sapphire or silicon substrate should be removed. Hence, the device in our study is considered as a vertical structure, with the positive and negative electrodes located above and below an active layer, respectively. The schematic diagram is shown in **Figure 1**. The vertical structure can also avoid the influence of the current crowding effect. The device structure consists of a 3 μm-thick n-GaN layer with Si doping concentration of 5×10^{18} cm^{-3} and a slightly doped single-period 3 nm $In_{0.18}Ga_{0.85}N$/10 nm GaN quantum well (QW). The GaN spacer with a thickness of 15 nm above the QW is considered, followed by a 20 nm p-$Al_{0.15}Ga_{0.85}N$ layer as the electron blocking layer (EBL) and 200 nm p-GaN layer. The doping concentrations of EBL and p-GaN are set to 1.2×10^{19} cm^{-3}.[15,20] It should be mentioned that, due to the N vacancies and O impurities, the unintentionally doped GaN has high background carrier concentration.[21] Hence the QW and GaN barrier are set to have a slightly doped donor level of about 2×10^{18} cm^{-3}. ATLAS simulator (Silvaco) is used to perform device simulation, by solving Poisson's equation and carrier continuity equation based on a series of physical models. All μ-LEDs have the same parameters, except for the chip size. The Shockley–Red–Hall (SRH) recombination lifetime of the carriers is set to 1×10^{-7} s.[15] The radiative recombination coefficient B and the Auger recombination coefficient C are set to 2.1×10^{-11} and 1×10^{-30} cm^3 s^{-1}, respectively.[14,15] The band offset ratio, $\Delta E_c/\Delta E_v$ is set to 70:30.[15] The surface recombination velocity is set to 5×10^4 cm s^{-1}.[18]

The parameters of surface states must be carefully selected. The calculations based on density functional theory (DFT) show that the *m*-plane of GaN consists of buckled Ga–N dimer aligned along the [0001] direction in the outermost layer, which has an energy-stable and unreconstructed surface feature.[22] The dangling bonds of the Ga atoms and N atoms introduce surface states named S_{Ga} and S_N, respectively. The energy of S_{Ga} is close to the conduction band minimum (CBM) and has a dispersion, which makes the surface states energy extend toward the middle of the bandgap. Furthermore, the unoccupied S_{Ga} states give rise to the pinning of the Fermi level at GaN *m*-plane, which leads to an upward surface band bending with about 0.6 eV.[23,24]

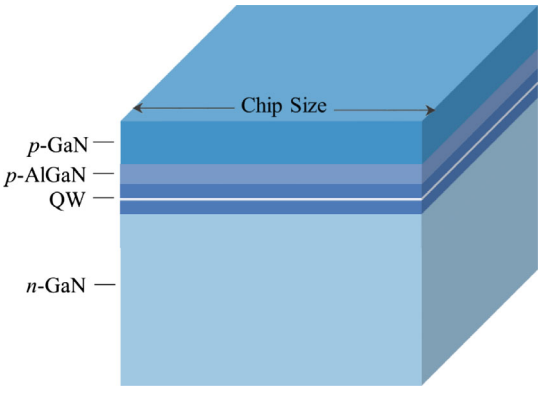

Figure 1. The schematic diagram of the μ-LED device structure.

Considering the earlier reasons, the surface states were introduced into the μ-LED model. The density of the surface states is set to 1×10^{14} cm^{-2} with a capture cross section of 2×10^{-15} cm^{-2} based on the reported experimental values.[15,25]

First, the effect of surface states on the energy band near the surface is investigated. Due to the energy difference between the bulk Fermi level and surface states, electrons could diffuse to the surface and occupy the Ga dangling bonds, leading to the surface depletion region and making the surface band bending upward. Meanwhile, electrons in the surface depletion region are driven by the depletion field and drift from surface to the bulk, to form a dynamic equilibrium state. The depletion width was calculated using the drift-diffusion transport model incorporating the states of surface dangling bonds.[26] For the equilibrium state of μ-LEDs with a size of 1 μm, the energy band of the QW along the [1$\bar{1}$00] direction is shown in **Figure 2**a. The results show the upward band bending (V_{bb}) with 0.6 eV at the surface and the surface depletion region with a depth of about 40 nm. At zero bias, the surface band bending is caused by the transfer process of electrons which occupy the unoccupied Ga dangling bond, giving rise to the pinning of the Fermi level at the surface. The calculated results are consistent with the experimentally reported values in GaN nanostructures.[27,28] As carreir density increases, the electronic quasi-Fermi energy level moves upward and the surface states below the electron quasi-Fermi level are occupied.

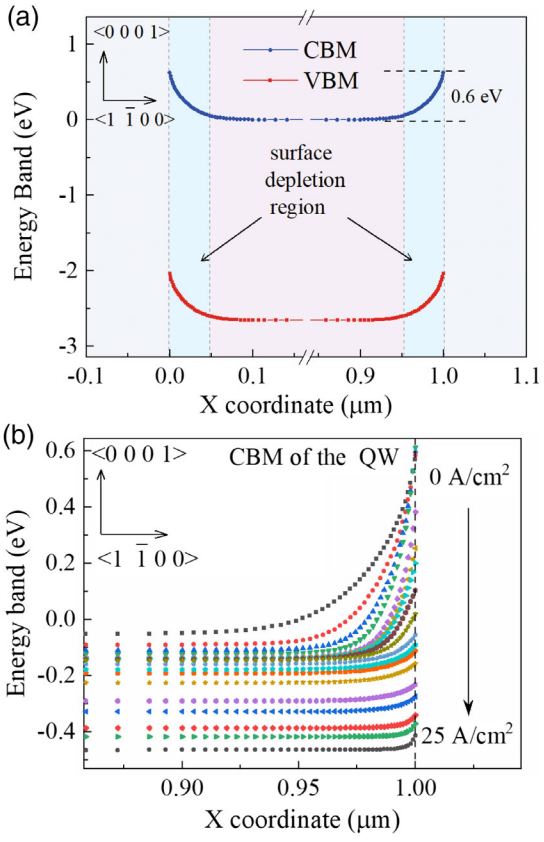

Figure 2. a) The cross-section view for the band structure conduction band minimum (CBM) and valence band maximum (VBM) of the QW at equilibrium state. b) The cross-section view for the band structure of the QW with current density from 0 to 25 A cm^{-2}.

Finally, it results in the reduction of V_{bb} as well as the depth of the surface depletion region, as shown in Figure 2b. Interestingly, at the beginning of the current density's increase, V_{bb} does not change, whereas the surface depletion depth decreases. Then, as the current denisty increases further, the V_{bb} shows a significant decrease. At the current density of 5.6 A cm^{-2}, V_{bb} and the surface depletion depth decrease to 47 meV and about 10 nm, respectively.

The relationship between V_{bb} and current density is shown in **Figure 3**a. V_{bb} decreases with increasing current density and then increases with the adversative point. The adversative position of V_{bb} shifts to a higher current density with decreasing size. A similar shift occurs in the current density of the peak IQE. As the current density increases further from the adversative point, band bending starts to increase again. When voltage is not applied to a device, the electrons occupying the surface make it negatively charged, resulting in upward band bending with 0.6 eV in our case. As carriers begin to inject into the QW, holes in the surface depletion region drift to the surface and compensate a part of the negative surface charges, casusing the reduction of upward band bending. With a current density higher than the adversative point, due to higher electron injection of GaN-based μ-LEDs, more electrons flow into the QW and occupy the surface.[29] The total amout of the negative surface charges starts to increase and it results in upward band bending again. For all the μ-LED devices, the minimum values of V_{bb} are about 45 meV.

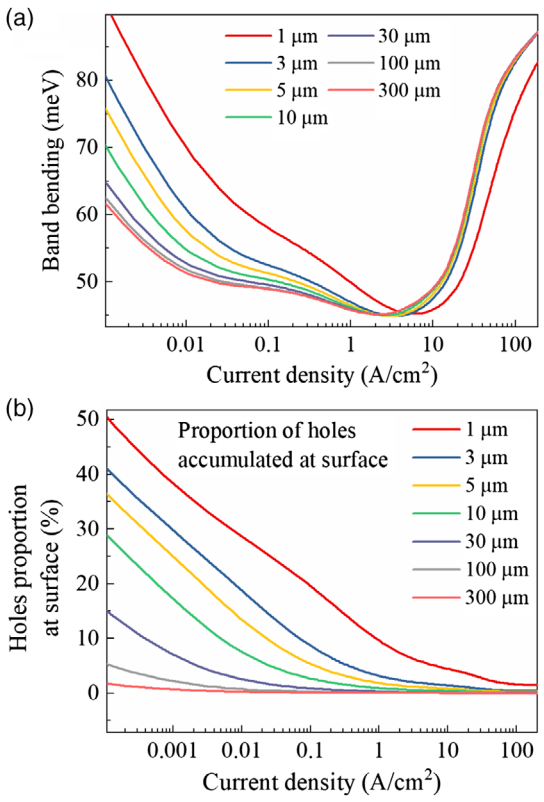

Figure 3. a) The surface band bending varied with current density. b) The proportion of holes accumulated on the surface varied with the current density.

Due to the upward bending of the surface energy band, holes redistribute near the surface. In μ-LEDs, holes tend to accumulate near the surface, leading to nonraidative surface recombination. So, the hole accumulation behavior is quantitatively analyzed at the surface with the depth of 6 nm, as shown in Figure 3b. The depth is extracted from the surface depletion region with current density at the peak IQE. Then, the holes proportion was calculated by dividing the number of holes in the surface depletion region by the number of holes in the QW. The result shows that the hole ratio at the surface decreases as the current density increases. From the results, as the current density increases, the accumulated holes at the surface reach the maximum level and the rest of the holes tend to stay in the bulk. Thus, the ratio of the surface holes to the total holes in the QWs decreases. In particular, the hole accumulation is more significant for μ-LEDs with a size of less than 10 μm. μ-LEDs in microdisplays have to operate at a low current density (<20 A cm^{-2}). Thus, this expected to make the device performance of μ-LEDs worse with decreasing size.

The hole accumulation at the surface of InGaN multiple quantum well (MQW) LED is experimentally confirmed using the wet etching of LED micropillars. The wet etching of nitride materials involves oxidation of the semiconductor surface and the subsequent dissolution of the resulting oxides. The oxidation process requires the involvement of only holes at the surface, which can be strong evidence for the accumulation of holes at the surface. The relevant chemical reaction can be expressed as

$$2GaN + 6oH^- + 6h^+ \rightarrow Ga_2O_3 + 3H_2O + N_2 \quad (1)$$

In chemical etching without electrical contact, the holes are usually supplied by the photon energy higher than the bandgap or by adding the oxidizing agent, which depletes valence band electrons and generate holes at the surface. However, in our experiment, wet etching is conducted in KOH solution (2 mol L^{-1}, 80 °C) without UV illumination and an oxidizing agent. Therefore, the etching speed is dependent on only hole concentration at the surface of the LED device. Higher hole accumulation leads to a higher etching rate by the fast oxidation process. Thus, the area of LEDs with higher hole concentration at the surface is expected to have a deeper etch depth. The commericial LED wafer (Changelight Co., Ltd) is used and the detailed LED structure used for the experiment can be seen in the Experimental Section. The LED micropillars are prepared by photolithography and subsequent etching processes. **Figure 4**a shows the scanning electron microscopy (SEM) image of the trapezoid-shaped LED pillar array after fabrication, i.e., no etching process. The top diameter and height of each pillar are ≈2 and ≈1.2 μm, respectively. After 40 min of etching in KOH, the sidewall of the pillar becomes vertical due to the anisotropy of etching on different crystal plane, as shown in Figure 4b. After 2 h of etching in KOH, the pillar shape is further changed by the different etching depths casued by the different hole concentrations on the sidewall of the pillar, as shown in Figure 4c,d. The SEM image of the single LED pillar in Figure 4d shows that the bottom side of the pillar has a more deeper etching depth due to higher hole concentration. As expected, it shows that the diameter of n-GaN and MQWs is smaller than that of p-GaN, which indicates that the etching rates for n-GaN and MQWs are larger

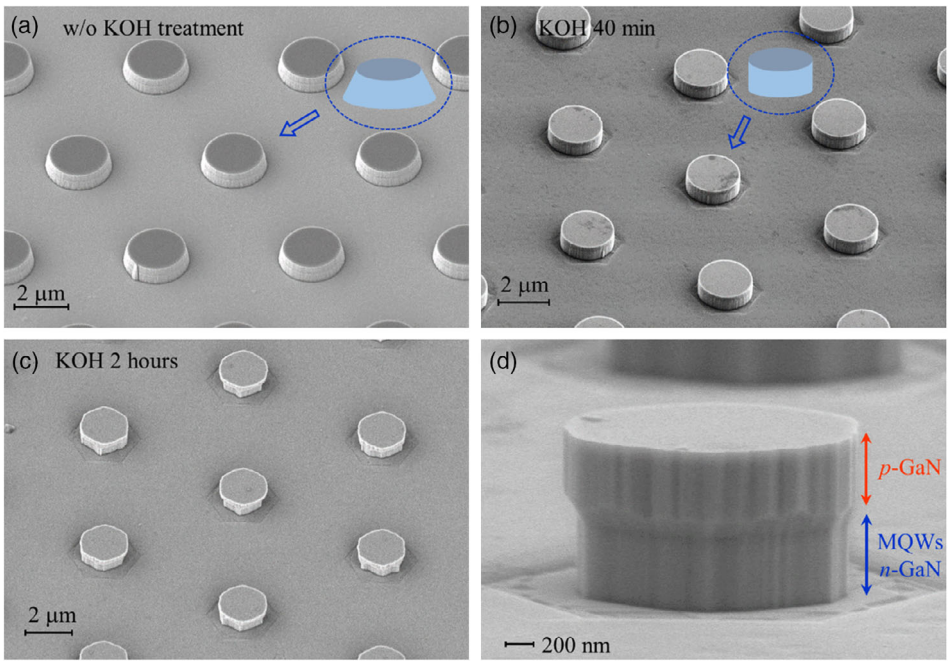

Figure 4. a–c) SEM images of the LED micropillars without wet etching (a), after 40 min etching in KOH (b), and after 2 h etching in KOH (c). d) The SEM image of the single pillar after 2 h etching in KOH.

than that of p-GaN. The morphology change of the LED micropillars by wet etching is key evidence for hole accumulation at the surface of the active layer of InGaN μ-LEDs.

The calculated hole concentrations near the nonpolar surface for the 1 μm μ-LED with current density of 12.5 A cm^{-2} are shown in **Figure 5**a. In the QW, due to the polarized electric field, the holes distribute near the GaN barrier. The hole concentration at the surface is higher than that in the bulk for both the QW and GaN barrier. The hole concentration at the surface of QW is about 4.3×10^{18} cm^{-3} whereas that in the bulk QW is about

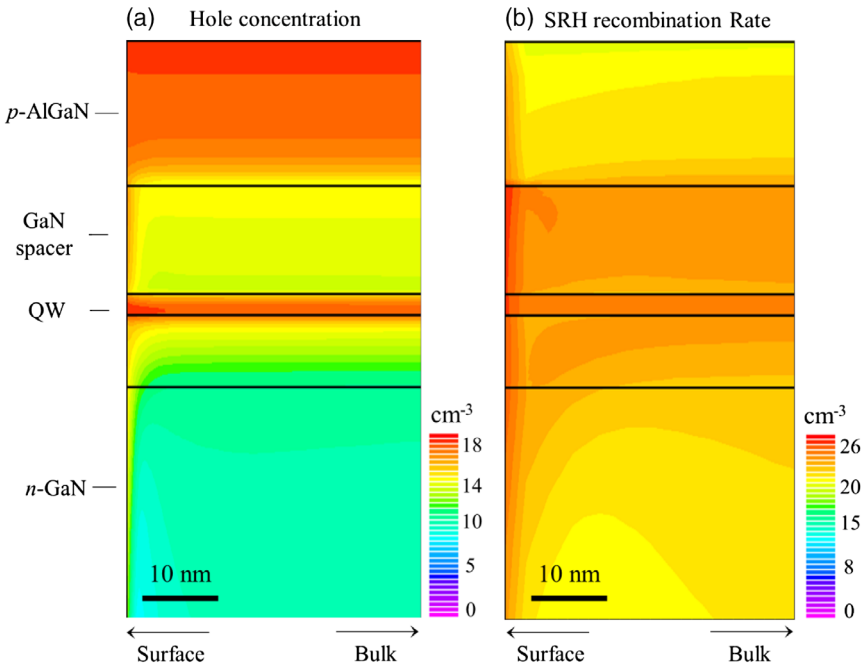

Figure 5. a) The cross-section view for the hole concentration with current density of 12.5 A cm^{-2}. b) The cross-section view for SRH recombination rate with current density of 12.5 A cm^{-2}. (The color level is displayed with 10^x scale).

3.5×10^{17} cm^{-3}. Due to the hole accumulation at the surface, a significant nonradiative recombination could occurr near the surface region with a depth of 6 nm, as shown in Figure 5b. In addition to the QW, significant surface recombinaiton also occurs at the GaN barrier.

Now, let us turn our attention to the effect of nonradiative recombination near the surface on the IQE of μ-LEDs. IQEs are calculated for μ-LEDs with size between 1 and 300 μm as a function of curent density, as shown in **Figure 6**a. The IQE is obtained by dividing the integration of radiative recombination in the QW with that of the recombination in μ-LEDs. As the size decreases from 300 to 30 μm, the IQE only decreases from 57.7% to 51.3%, whereas the peak current density shifts from 14.7 to 15.1 A cm^{-2} (Figure 6b). In this size range, the hole proportion at the surface on the peak current density is less than 0.02%, as shown in Figure 3b. Therefore, the change of IQEs and the shift of the peak current density are negligible, i.e., almost size independent, which is consistent with the reported experimental results.[7] In the size range from 30 to 10 μm, the IQE starts to exhibit an obvious attenuation, from 51.3% to 40.9%, whereas the peak current density only increases from 15.1 to 15.6 A cm^{-2}. Significant change occurs in the size range from 10 to 1 μm. The IQE decreases from 40.9% to 10.1% whereas the peak current density increases from 15.6 to 21.9 A cm^{-2}. In this region, μ-LEDs show the size-dependent feature. It is worth noting that the surface damage is not considered in our model. Hence, in this region, the efficiency attenuation and the shift of the peak current density are entirely caused by the nonradiative surface recombination that originates from the intrinsic surface property.

The study with the GaN-based nanowire LEDs shows that the surface band bending causes carrier redistribution and largely affects carrier injection efficiency, giving the similar result shown in Figure 3b.[25] As the μ-LED size decreases, the hole accumulation at the surface becomes more serious. The accumulated holes due to the upward bending of the surface energy band have a great influence on the IQE and peak current density, especially for the μ-LEDs with a size ≤10 μm. In **Figure 7**, the extracted V_{bb} varying with current density shows clearly that the minimum V_{bb} (white line) increases to a higher current density with decreasing size. In the size range from 3 to 1 μm, the minimum V_{bb} shows significant movement toward a higher current density. The peak current densities are marked with red stars, showing that the variation tendency of the peak current density is similar to that of band bending.

Based on our results, the effect of the intrinsic surface property on the efficiency of μ-LEDs is proposed in the schematic diagram of **Figure 8**. The dangling bonds of the Ga and N atoms form two surface bands with the energy close to the CBM and VBM, respectively.[22–24] The previous calculation shows that, due to different electronegativities, charge tranfers from the Ga atoms to the N atoms, causing S_N to be occupied and S_{Ga} to be unoccupied, give rise to the Fermi energy to be pinned at GaN *m*-plane.[23] Furthermore, S_N could be resonant with the bulk valence band at the $\bar{\Gamma}$ point, which offers transition posibility between the electrons occupied on S_N and the holes located beside the surface.[22] As the carrier is injected into the QW, holes are driven by the surface depletion field and drift to the surface region, causing nonradiative recombination with the electrons occupied on the N-deprived states. The asymmetric carrier injection and transport of GaN-based LEDs have been well known as the bottlenecks for improving device performance.[29] The large ionization energy of the dopant Mg causes hole concentration to be lower than that of electrons.[30] Therefore, hole accumulation and nonradiative recombination at the surface further deteriorate the device performance and result in a significant efficiency loss on μ-LEDs with

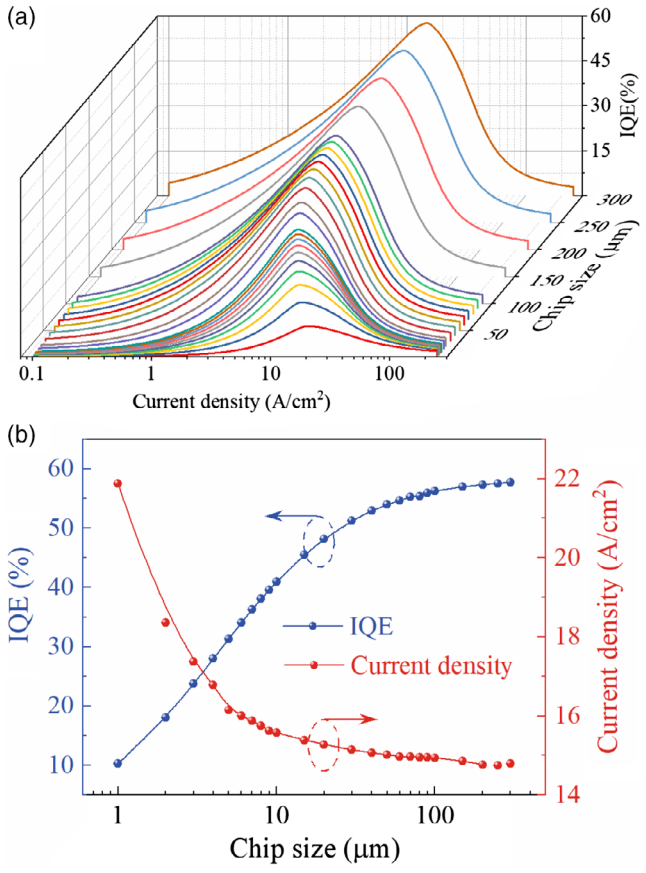

Figure 6. a) The IQE of the μLEDs with size from 1 to 300 μm as a function of current density. b) The maximum IQE and the peak current density versus the μLEDs size.

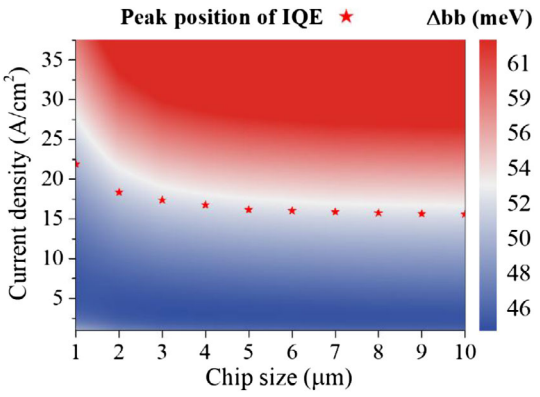

Figure 7. The surface band bending value versus the current density for the μLED with size from 1 to 10 μm, and the current density for the peak IQE is marked as stars.

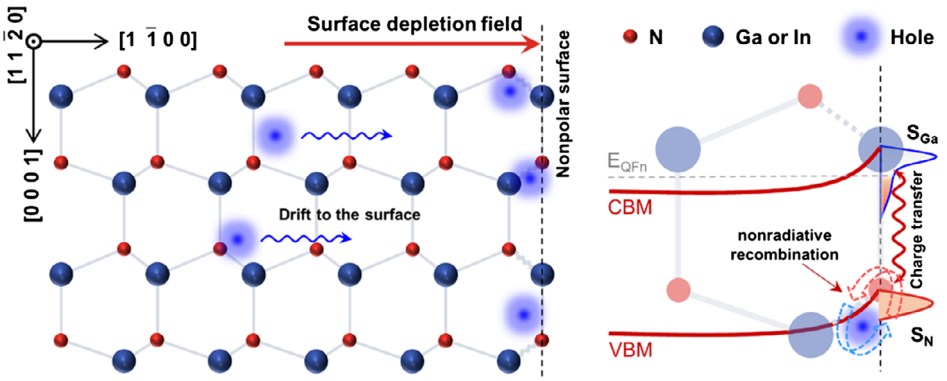

Figure 8. The schematic diagram of surface recombination model.

size less than 10 μm. Therefore, surface band engineering, which is used in water splitting with group-III nitride nanostructure, could be required to improve the efficiency of small-sized μ-LEDs accompanying surface passivation.[31]

The influence of the intrinsic surface for GaN-based μ-LEDs is investigated to illustrate the efficiency attenuation behavior in small-sized μ-LEDs. Our results strongly indicate that hole accumulation due to the upward bending of the surface energy band is the main physical mechanism for nonradiative recombination between the electrons occupied at N atoms of the surface and holes at the surface. This results in a significant efficiency loss in μ-LEDs with size $\leq$10 μm. Thus, we propose the passivation with purposive surface energy band engineering in the μ-LED fabrication process to improve the device performance of small-sized GaN-based μ-LEDs.

Experimental Section

The commercial-grade blue LED wafer from Changelight Co., Ltd, was used for chemical etching. The LED structure is shown in **Figure 9**. First, 200 nm silicon oxide (SiO_2) was deposited using plasma-enhanced chemical vapor deposition (PECVD). A circle mesa with a diameter of 2 μm was defined by ICP to etch down through the SiO_2 to n-GaN. Finally, the SiO_2 layer was removed using buffered oxide etch (BOE) solution. Then, the sample was treated with KOH solution with 2 mol L^{-1} at 80 °C at different times.

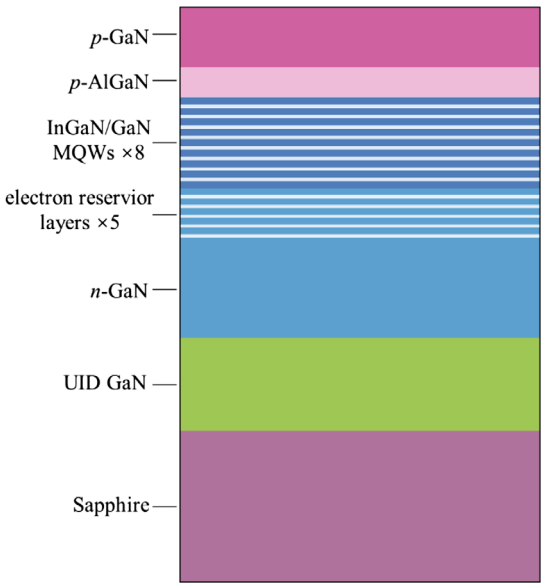

Figure 9. The cross-sectional schematic of the blue LED wafer.

Acknowledgements

This work was financially supported by Guangdong Science and Technology funding (project name: High Speed Visible Light Communications based on RGB Micro-LED Arrays, grant no. 2017B010114002), Shenzhen Science and Technology Program (grant no. KQTD20170810110313773), Shenzhen Technology Research Project (project name: Novel Mini-LED flexible transparent displays technology, grant no. JSGG20180507183058189), Key-Area Research and Development Program of GuangDong Province (grant no. 2019B010925001), and High-level University Fund G02236005. The authors declare that they have no competing financial interests.

Conflict of Interest

The authors declare no conflict of interest.

Keywords

GaN, internal quantum efficiency, micro-light-emitting-diodes, nonradiative surface recombination

Received: October 11, 2020
Revised: December 4, 2020
Published online: December 23, 2020

[1] Z. Liu, C.-H. Lin, B.-R. Hyun, C.-W. Sher, Z. Lv, B. Luo, F. Jiang, T. Wu, C.-H. Ho, H.-C. Kuo, J.-H. He, *Light: Sci. Appl.* **2020**, *9*, 83.
[2] Y. Huang, E.-L. Hsiang, M.-Y. Deng, S.-T. Wu, *Light: Sci. Appl.* **2020**, *9*, 105.
[3] J. Wierer, N. Tansu, *Laser Photonics Rev.* **2019**, *13*, 1900141.
[4] T. Wu, C.-W. Sher, Y. Lin, C.-F. Lee, S. Liang, Y. Lu, S.-W. Huang Chen, W. Guo, H.-C. Kuo, Z. Chen, *Appl. Sci.* **2018**, *8*, 1557.
[5] C. Vieri, G. Lee, N. Balram, S. H. Jung, J. Y. Yang, S. Y. Yoon, I. B. Kang, *J. Soc. Inf. Disp.* **2018**, *26*, 314.
[6] J. M. Smith, R. Ley, M. S. Wong, Y. H. Baek, J. H. Kang, C. H. Kim, M. J. Gordon, S. Nakamura, J. S. Speck, S. P. DenBaars, *Appl. Phys. Lett.* **2020**, *116*, 071102.

[7] M. S. Wong, C. Lee, D. J. Myers, D. Hwang, J. A. Kearns, T. Li, J. S. Speck, S. Nakamura, S. P. DenBaars, *Appl. Phys. Express* **2019**, *12*, 097004.
[8] J. Zhu, T. Takahashi, D. Ohori, K. Endo, S. Samukawa, M. Shimizu, X.-L. Wang, *Phys. Status Solidi A* **2019**, *216*, 1900380.
[9] P. Tian, J. J. D. McKendry, Z. Gong, B. Guilhabert, I. M. Watson, E. Gu, Z. Chen, G. Zhang, M. D. Dawson, *Appl. Phys. Lett.* **2012**, *101*, 231110.
[10] K. A. Bulashevich, S. Y. Karpov, *Phys. Status Solidi RRL* **2016**, *10*, 480.
[11] H. David, M. Asad, D. P. Christopher, N. Shuji, P. D. Steven, *Appl. Phys. Express* **2017**, *10*, 032101.
[12] F. Olivier, A. Daami, C. Licitra, F. Templier, *Appl. Phys. Lett.* **2017**, *111*, 022104.
[13] F. Olivier, S. Tirano, L. Dupre, B. Aventurier, C. Largeron, F. Templier, *J. Lumin.* **2017**, *191*, 112.
[14] S. S. Konoplev, K. A. Bulashevich, S. Y. Karpov, *Phys. Status Solidi A* **2018**, *215*, 1700508.
[15] J. Kou, C.-C. Shen, H. Shao, J. Che, X. Hou, C. Chu, K. Tian, Y. Zhang, Z.-H. Zhang, H.-C. Kuo, *Opt. Express* **2019**, *27*, A643.
[16] M. S. Wong, D. Hwang, A. I. Alhassan, C. Lee, R. Ley, S. Nakamura, S. P. Denbaars, *Opt. Express* **2018**, *26*, 21324.
[17] P. Morgan Pattison, M. Hansen, J. Y. Tsao, *C. R. Phys.* **2018**, *19*, 134.
[18] R. Aleksiejūnas, M. Sūdžius, T. Malinauskas, J. Vaitkus, K. Jarašiūnas, S. Sakai, *Appl. Phys. Lett.* **2003**, *83*, 1157.
[19] V. M. Kaganer, J. Lähnemann, C. Pfüller, K. K. Sabelfeld, A. E. Kireeva, O. Brandt, *Phys. Rev. Appl.* **2019**, *12*, 054038.
[20] Silvaco, Blue LED Simulation, https://silvaco.com/simulation-standard/blue-led-simulation/, (accessed: December 2020).
[21] T. T. Zhu, R. A. Oliver, *Phys. Chem. Chem. Phys.* **2012**, *14*, 9558.
[22] M. Landmann, E. Rauls, W. G. Schmidt, M. D. Neumann, E. Speiser, N. Esser, *Phys. Rev. B* **2015**, *91*, 035302.
[23] M. Himmerlich, A. Eisenhardt, S. Shokhovets, S. Krischok, J. Räthel, E. Speiser, M. D. Neumann, A. Navarro-Quezada, N. Esser, *Appl. Phys. Lett.* **2014**, *104*, 171602.
[24] L. Lymperakis, J. Neugebauer, M. Himmerlich, S. Krischok, M. Rink, J. Kröger, V. M. Polyakov, *Phys. Rev. B* **2017**, *95*, 195314.
[25] S. Zhang, A. T. Connie, D. A. Laleyan, H. P. T. Nguyen, Q. Wang, J. Song, I. Shih, Z. Mi, *IEEE J. Quantum Electron.* **2014**, *50*, 483.
[26] S. Selberherr, *Analysis and Simulation of Semiconductor Devices*, Springer-Verlag, Vienna, Austria **1984**.
[27] B. S. Simpkins, M. A. Mastro, C. R. Eddy Jr., P. E. Pehrsson, *J. Appl. Phys.* **2008**, *103*, 104313.
[28] R. Calarco, T. Stoica, O. Brandt, L. Geelhaar, *J. Mater. Res.* **2011**, *26*, 2157.
[29] J. Cho, E. F. Schubert, J. K. Kim, *Laser Photonics Rev.* **2013**, *7*, 408.
[30] G. Verzellesi, D. Saguatti, M. Meneghini, F. Bertazzi, M. Goano, G. Meneghesso, E. Zanoni, *J. Appl. Phys.* **2013**, *114*, 071101.
[31] M. G. Kibria, S. Zhao, F. A. Chowdhury, Q. Wang, H. P. T. Nguyen, M. L. Trudeau, H. Guo, Z. Mi, *Nat. Commun.* **2014**, *5*, 3825.